Design of Feature Extraction Operators for use on Biologically Motivated Hexagonal Image Structures

[1]Sonya Coleman, [2]Bryan Scotney, [1]Bryan Gardiner
[1]*University of Ulster, Magee, BT48 7JL, Northern Ireland*
[2]*University of Ulster, Coleraine, BT52 1SA, Northern Ireland*
{sa.coleman, bw.scotney}@ulster.ac.uk
gardiner-b@email.ulster.ac.uk

Abstract

For many years the concept of using hexagonal pixels for image capture has been investigated, and several advantages of such an approach have been highlighted. Recently there has been a renewed interest in the use of hexagonal images: biologically inspired approaches, representation of architectures for such images and general hexagonal image processing. We present multi-scale hexagonal gradient operators that are developed within the finite element framework for use directly on hexagonal pixel-based images. We evaluate the proposed operators using simulated hexagonal images and provide performance evaluation using the Figure of Merit technique for comparison with existing hexagonal gradient operators.

1. Introduction

Image processing tasks have traditionally involved the use of square operators on rectangular image lattices. A more recently explored concept is the use of hexagonal pixels for image representation, introducing the area of hexagonal image processing. A prominent factor that merits the investigation of the hexagonal lattice as an alternative grid structure for image representation is its similarity to the human fovea. In order for humans to process visual input, the eye captures information that is directed to the retina located on the inner surface of the eye. A small region within the retina, known as the fovea and consisting of a high density of cones, is responsible for sharp vision capture and is comprised of cones that are shaped and placed in a hexagonal arrangement [4,7,10], as shown in Figure 1. This hexagonal mosaic provides the motivation to investigate an alternative grid structure for image representation other than rectangular.

In addition to replicating the characteristics of the human eye, hexagonal grids have other advantages over the conventional rectangular grid. Equidistance of all pixel neighbours facilitates the implementation of circular symmetric kernels that is associated with an increase in accuracy when detecting edges, both straight and curved [2], and the improved accuracy of circular and near circular image processing operators has been demonstrated in [3]. Additionally, better spatial sampling efficiency is achieved by the hexagonal structure compared with a rectangular grid of similar pixel separation, leading to improved computational performance. In a hexagonal grid with unit separation of pixel centres, approximately 13% fewer pixels are required to represent the same image resolution as required on a rectangular grid with unit horizontal and vertical separation of pixel centres [14].

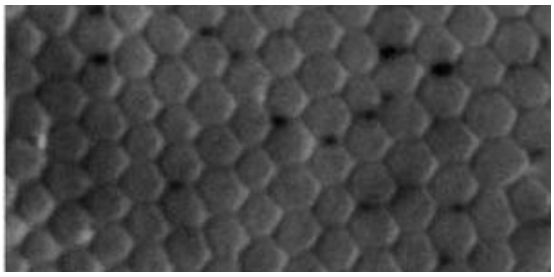

Figure 1. Cross section of human retina showing the hexagonal structure of the photoreceptor cones densely packed in the fovea [4]

Our work is motivated by recent work that uses the hexagonal structure, including biologically inspired fovea modelling with neural networks that correspond to the hexagonal biological structure of photoreceptors [8], and the development of silicon retinas for robot vision [13]. Image representation in a hexagonal structure can be achieved currently through rectangular to hexagonal image conversion [16], though the emergence of genuine hexagonal-based sensor systems and image capture devices is essential for the benefits of hexagonal structure to be fully appreciated and exploited, and camera sensor manufacturers are starting to build cameras that approximate a hexagonally based sensor structure; for example, Fuji have developed the FujiFilm FinePix S3 pro.

In this paper, we present a novel approach to the design of hexagonal image processing operators, implementing the approach in [16] to obtain hexagonal images. In Section 2 we present our multi-scale operator design, with performance evaluation using simulated hexagonal images presented in Section 3. Section 4 provides a summary and details of further work.

2. Multi-scale hexagonal operator design

We represent the hexagonal pixel-based image by using an array of samples of a continuous function $u(x, y)$ of image intensity on a domain Ω. Figure 2 represents hexagonal pixels with a node placed in the centre of each pixel. These nodes are the reference points for the computation of finite element techniques throughout the domain Ω.

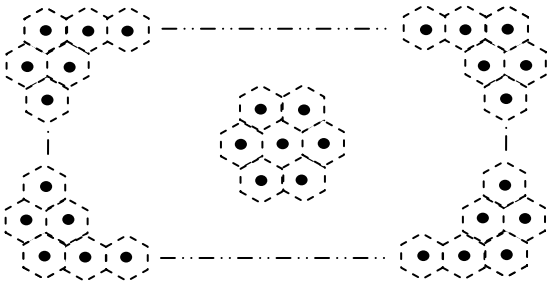

Figure 2. Representation of a hexagonal image

The multi-scale operators designed specifically for use on the image represented in Figure 2 are based on the use of a mesh, illustrated in Figure 3, consisting of equilateral triangular elements which overlays the pixel array shown in Figure 2.

With any node in the mesh, say node i, with co-ordinates (x_j, y_j) we associate a piecewise linear basis function $\phi_i(x, y)$ which has the properties $\phi_i(x_j, y_j) = 1$ if $i = j$ and $\phi_i(x_j, y_j) = 0$ if $i \neq j$, where (x_j, y_j) are the co-ordinates of the nodal point j. $\phi_i(x, y)$ is thus a "tent-shaped" function with support restricted to a small neighbourhood centred on node i consisting of only those triangular elements that have node i as a vertex. We then may approximately represent the image u over the neighbourhood Ω_i^σ by a function

$$U(x, y) = \sum_{j \in D_i^\sigma} U_j \phi_j(x, y)$$

in which the parameters $\{U_j\}$ are mapped from the hexagonal image intensity values; thus the approximate image representation is a simple piecewise linear function on the triangular elements in the neighbourhood Ω_i^σ and having intensity values $\{U_j\}$ at nodes j.

The operators are formulated such that they correspond to weak forms in the finite element method. As we are currently concerned only with first order derivative operators, a weak form of the first directional derivative $\delta u / \delta b \equiv \underline{b} \cdot \underline{\nabla} u$ is obtained by multiplying the derivative term by a test function $v \in H^1$ and integrating on the image domain Ω to give $(u) = \int_\Omega \underline{b} \cdot \underline{\nabla} u v d\Omega$, where $\underline{b} = (\cos\theta, \sin\theta)$ is the unit direction vector. This approach enables us to design our hexagonal operator using either a Cartesian coordinate system or the three axes of symmetry of the hexagon. Our current operator design uses the Cartesian system as use of the three axes of symmetry introduces redundancy. However, the hexagonal coordinate system has advantages when applied to tasks such as rotation that involve a large degree of symmetry [15], and hence may be used in future work

In the finite element method a finite-dimensional subspace $S^h \subset H^1$ is used for function approximation; in our design procedure S^h is defined by the finite element mesh in Figure 3. Our general design procedure incorporates a finite-dimensional test space $T_\sigma^h \subset H^1$ that explicitly embodies a scale parameter σ and this test space T_σ^h comprises a set of Gaussian basis functions $\psi_i^\sigma(x, y)$, $i = 1, .., N$ of the form

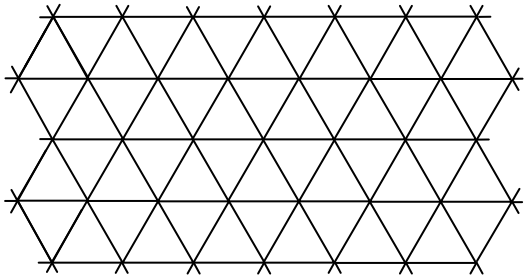

Figure 3. Mesh of equilateral triangle elements

$$\psi_i^\sigma(x, y) = \frac{1}{2\pi\sigma^2} e^{-\left(\frac{(x-x_i)^2 + (y-y_i)^2}{2\sigma^2}\right)}.$$

Each test function is restricted to have support over the neighbourhood, centred on node i. In general the size of Ω_i^σ may be explicitly related to the scale parameter σ [12], as illustrated by the six-element and 24-element hexagonal neighbourhoods in Figure 4. The sets of test functions $\psi_i^\sigma(x, y)$, $i = 1, \ldots, N$, are then used in the weak forms of the first derivative, providing the functional $E_i^\sigma(U) = \int_{\Omega_i^\sigma} \underline{b} \cdot \underline{\nabla} \psi_i^\sigma d\Omega_i$. We should note that the integrals need to be computed only over the neighbourhood Ω_i^σ, rather than the entire image domain Ω, since ψ_i^σ has support restricted to Ω_i^σ.

To illustrate the implementation of the first order hexagonal operator, the general equilateral triangular element, as shown in Figure 5, will be used. Here one of the nodes α, β, λ is a central node i of a neighbourhood. For example, the neighbourhood Ω_i^σ, in Figure 4(a) covers a set of 6 elements $\{e_m\}$; where a Gaussian basis function ψ_i^σ is associated with the central node i which shares common support with the surrounding seven basis functions ϕ_i. Hence $E_i^\sigma(U)$ needs to be computed over the six elements in the neighbourhood Ω_i^σ. Substituting the image representation into the functional $E_i^\sigma(U)$ yields

$$E_i^\sigma(U) = b_{i1} \sum_{j=1}^{N} K_{ij}^\sigma U_j + b_{i2} \sum_{j=1}^{N} L_{ij}^\sigma U_j$$

where $K_{ij}^\sigma = \sum_{m | e_m \in S_i^\sigma} k_{ij}^{m,\sigma}$ and $L_{ij}^\sigma = \sum_{m | e_m \in S_i^\sigma} l_{ij}^{m,\sigma}$ and $k_{ij}^{m,\sigma}$ and $l_{ij}^{m,\sigma}$ are the element integrals

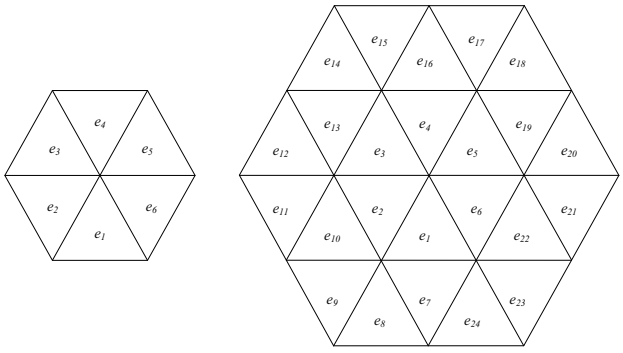

(a) (b)

Figure 4. Hexagonal operator structures: (a) six-element neighbourhood; (b) 24-element neighbourhood

$k_{ij}^{m,\sigma} = \int \frac{\delta \emptyset_i}{\delta x} \psi_i^{\sigma} dxdy$ and $l_{ij}^{m,\sigma} = \int \frac{\delta \emptyset_i}{\delta y} \psi_i^{\sigma} dxdy$.

In order to calculate and $k_{ij}^{m,\sigma}$ and $l_{ij}^{m,\sigma}$, a local co-ordinate reference system for an equilateral triangle is introduced as illustrated in Figure 5, with co-ordinates ξ and η such that $\xi \geq 0, \eta \geq 0$ and $1 - \xi - \eta \geq 0$. A mapping of these global co-ordinates to local co-ordinates can be obtained by means of a co-ordinate transformation from e_m to $\hat{e}$ defined by $x = (x_2^m - x_1^m)\xi + (x_3^m - x_1^m)\eta + x_1^m$ and $y = (y_2^m - y_1^m)\xi + (y_3^m - y_1^m)\eta + y_1^m$.

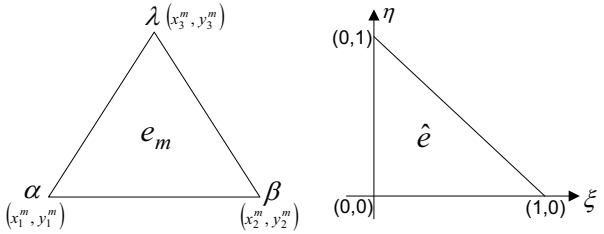

Figure 5. Local co-ordinate transformation

3. Comparative results

To process and evaluate hexagonal pixel-based images we create an environment that simulates the use of a hexagonal image sensor. We initially create hexagonal pixel-based images using clusters of rectangular sub-pixels as in [16] in order to compare our proposed approach of multi-scale hexagonal gradient operators with other existing gradient operators that can be used directly on hexagonal pixel-based images, namely the modified Sobel and Prewitt hexagonal operators and the operator proposed by Davies [5]. Using these resampled hexagonal images, processing and evaluating can be implemented in a hexagonal environment, as illustrated in Figure 6.

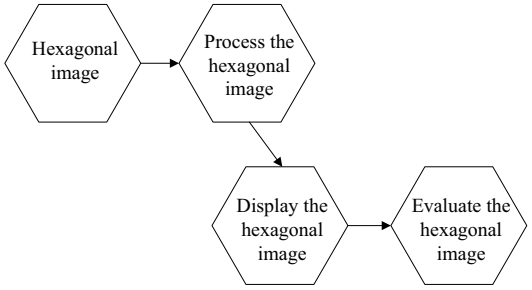

Figure 6. Processing hexagonal images

In order to accurately measure the performance of hexagonal gradient operators, the well-known Figure of Merit technique [1] was modified to accommodate the use of hexagonal pixel-based images. Comparison was made directly on the simulated hexagonal images between the proposed hexagonal operators of size 3×3, 5×5 and 7×7 (denoted H3, H5 and H7 respectively) and with existing hexagonal Prewitt, Sobel and Davies operators (denoted as P, S and D respectively). The results presented in Figure 7 illustrate that our multi-scale approach is comparable with the existing hexagonal image processing operators. In particular, on the oriented and vertical edges, H3 provides improved results over the other equivalent 3×3 operators, with the larger scale operators (H5 and H7) performing significantly better in areas of high signal-to-noise ratio, as would be expected.

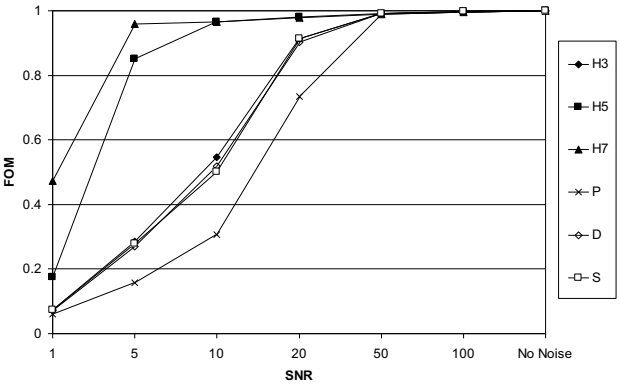

(a) FoM computed on an oriented edge 60^0

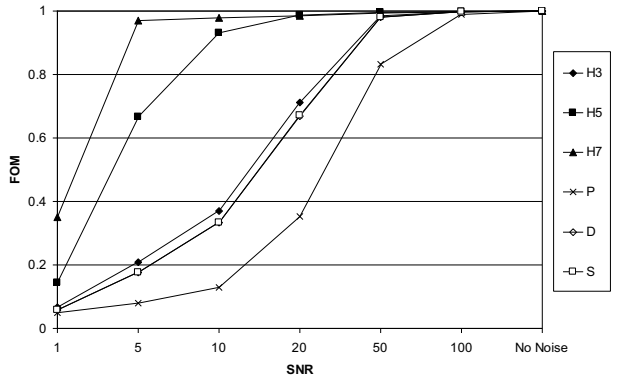

(b) FoM computed on a vertical edge

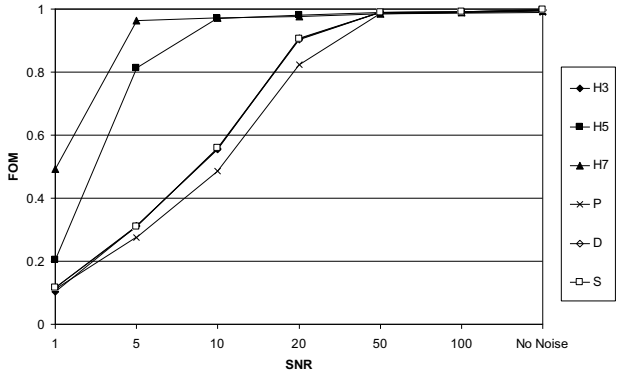

(c) FoM computed on a curved edge

Figure 7. Figure of Merit results

For further comparison we provide edge maps for each of the hexagonal operators previously evaluated, using the clock image shown in Figure 8. We obtain the hexagonal pixel-based images by re-sampling the original rectangular pixel-based image using the approach of [16], and the edge maps are presented in Figure 8, where, for each operator, we have chosen the visually best edge map (at the given threshold of **T**). As expected from obtained FoM results in Figure 7, the performance of H3 is comparable with the other 3x3 equivelent operators, where H5 and H7 demonstrate increased performance, in particular along the back edge of the clock.

4. Summary

The use of hexagonal pixel-based images has received

much attention in recent years with respect to both image architecture and, to a lesser extent, processing. Through the use of the finite element framework, we have presented a design procedure for multi-scale gradient operators developed explicitly for use on hexagonal pixel-based images. Using the Figure of Merit evaluation technique, we have demonstrated that the proposed operators detect edges more accurately than existing operators for processing hexagonal images, particularly in images with high signal-to-noise ratios; we have also illustrated satisfactory visual results via the use of a (re-sampled) real image. Further work will entail extending the operator design procedure to encompass the spiral architecture in [11].

Bibliography

[1] Abdou, I.E. and Pratt, W.K., "Quantitative Design and Evaluation of Enhancement/Thresholding Edge Detector", Vol. 67, pp. 753-763, 1979.

[2] Allen, J. D., "Filter Banks for Images on Hexagonal Grid", Signal Solutions, 2003.

[3] Coleman, S.A., Scotney, B.W., Herron, M.G., "A Systematic Design Procedure for Scalable Near-Circular Laplacian of Gaussian Operators", 17th International Conference on Pattern Recognition ICPR'04, Vol. 1, pp. 700 – 703, 2004.

[4] Curcio, C.A., et al., "Human Photoreceptor Topography", Journal of Comparative Neurology, Vol. 292, pp. 497-523, 1990.

[5] Davies, E.R. "Optimising Computation of Hexagonal Differential Gradient Edge Detector", Electronics Letters, Vol. 27, pp. 1526-1527, 1991.

[6] Deering, M.F., "A Photon Accurate Model of the Human Eye", Proceedings of ACM SIGGRAPH, New York, NY, USA, Vol. 24, pp. 649-658, 2005.

[7] Hirsch, J. and Miller, W.H., "Does Cone Positional Disorder Limit Resolution?", Journal of the Optical Society of America A: Optics, Image Science, and Vision, Vol. 4, pp. 1481-1492, 1987.

[8] Huang, C-H., Lin, C-T., "Bio-Inspired Computer Fovea Model Based on Hexagonal-Type Cellular Neural Network", IEEE Trans Circuits and Systems, 54(1), pp35-47, Jan 2007.

[9] Middleton, L. and Sivaswamy, J., "Edge Detection in a Hexagonal-image Processing Framework", Image and Vision Computing, Vol. 19, pp. 1071-1081, 2001.

[10] Mollon, J.D. and Bowmaker, J.K., "The Spatial Arrangement of Cones in the Primate Fovea", Nature, Vol. 360, pp. 677-679, 1992.

[11] Middleton, L. and Sivaswamy, J., "Hexagonal Image Processing; A Practical Approach", Springer 2005.

[12] Scotney, B.W., Coleman, S.A. & Herron, M.G., "Device Space Design for Efficient Scale-Space Edge Detection", Proceedings of the International Conference on Computational Science (ICCS2002), Springer-Verlag, LNCS, 2002.

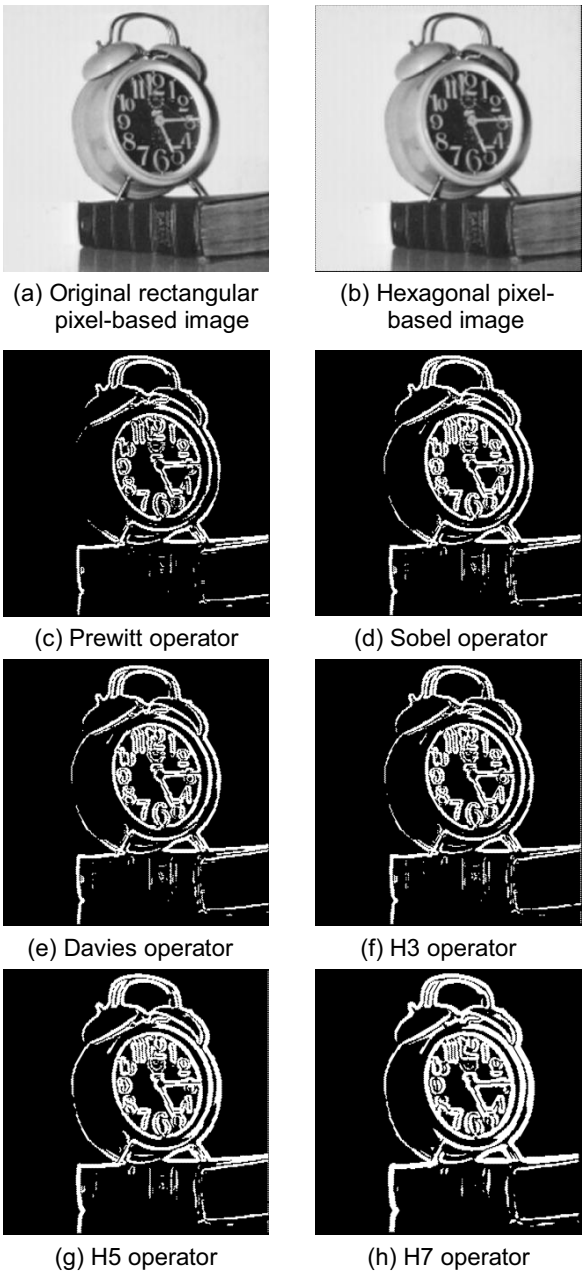

Figure 8. Real images and edge maps

[13] Shimonomura, K., et al., "Neuromorphic Binocular Vision System for Real-time Disparity Estimation", IEEE Int Conf on Robotics and Automation, pp.4867-4872, 2007.

[14] Vitulli, R., "Aliasing Effects Mitigation by Optimized Sampling Grids and Impact on Image Acquisition Chains," Geoscience and Remote Sensing Symposium, pp. 979-981, 2002.

[15] Wu, Q., He, X., Hintz, T., "Virtual Spiral Architecture," Int Conf on Parallel and Distributed Processing Techniques and Applications, pp. 339-405, 2004.

[16] Wuthrich, C.A, Stucki, P. "An Algorithmic Comparison Between Square-and Hexagonal-based Grid", CVGIP: Graphical Models and Image Processing, Vol. 53, pp. 324-339, 1999.